Meshless Local Petrov-Galerkin Method for Plane Piezoelectricity

J. Sladek[1], V. Sladek[1], Ch. Zhang[2], F. Garcia-Sanche[3], M. Wünsche[2]

Abstract: Piezoelectric materials have wide range engineering applications in smart structures and devices. They have usually anisotropic properties. Except this complication electric and mechanical fields are coupled each other and the governing equations are much more complex than that in the classical elasticity. Thus, efficient computational methods to solve the boundary or the initial-boundary value problems for piezoelectric solids are required. In this paper, the Meshless local Petrov-Galerkin (MLPG) method with a Heaviside step function as the test functions is applied to solve two-dimensional (2-D) piezoelectric problems. The mechanical fields are described by the equations of motion with an inertial term. To eliminate the time-dependence in the governing partial differential equations the Laplace-transform technique is applied to the governing equations, which are satisfied in the Laplace-transformed domain in a weak-form on small subdomains. Nodal points are spread on the analyzed domain and each node is surrounded by a small circle for simplicity. The spatial variation of the displacements and the electric potential are approximated by the Moving Least-Squares (MLS) scheme. After performing the spatial integrations, one obtains a system of linear algebraic equations for unknown nodal values. The boundary conditions on the global boundary are satisfied by the collocation of the MLS-approximation expressions for the displacements and the electric potential at the boundary nodal points. The Stehfest's inversion method is applied to obtain the final time-dependent solutions.

keyword: Meshless local Petrov-Galerkin method (MLPG), Moving least-squares interpolation, Piezoelectric solids, Coupled transient problem, Laplace-transform, Stehfest's inversion

1 Indroduction

Piezoelectric materials have wide range engineering applications in smart structures and devices. They are extensively utilized as transducers, sensors and actuators in many fields like telecommunications, robotics, microelectronics, mechatronics or adaptive intelligent structures. Piezoelectric effects were discovered in 1880 by J. and P. Curie. When a mechanical load is applied to a piezoelectric material an electrical voltage is generated. This phenomenon is known as the direct piezoelectric effect. On the contrary, an electrical voltage can produce a mechanical strain in a piezoelectric material, which is referred to as the inverse piezoelectric effect. Piezoelectric materials have usually anisotropic properties. Except this complication electric and mechanical fields are coupled each other and the governing equations are much more complex than that in the classical elasticity. Thus, efficient computational methods to solve the boundary or the initial-boundary value problems for piezoelectric solids are required. In spite of the great success of the finite element method (FEM) [Gaudenzi and Bathe (1995); Ha et al. (1992); Enderlein et al. (2005)] and the boundary element method (BEM) [Pan (1999); Lee (1995); Chen and Lin (1995); Ding and Liang (1999); Gross et al. (2005); Garcia-Sanchez et al. (2005, 2006); Sheng and Sze (2006)] as effective numerical tools for the solution of boundary or initial-boundary value problems in piezoelectric solids, there is still a growing interest in the development of new advanced methods. In recent years, meshless formulations are becoming popular due to their high adaptivity and low costs to prepare input and output data for numerical analysis. A variety of meshless methods has been proposed so far and some of them also applied to piezoelectric problems [Ohs and Aluru (2001); Liu et al. (2002)]. They can be derived either from a weak-form formulation on the global domain or a set of local subdomains. In the global formulation background cells are required for the integration of the weak-form. In methods based on local weak-form formulation no background cells are required and therefore they are often re-

[1] Institute of Construction and Architecture, Slovak Academy of Sciences, 84503 Bratislava, Slovakia

[2] Department of Civil Engineering, University of Siegen, D-57068 Siegen, Germany

[3] Department of Civil Engineering, University of Malaga, 29031 Malaga, Spain

ferred to as truly meshless methods. The meshless local Petrov-Galerkin (MLPG) method is a fundamental base for the derivation of many meshless formulations, since trial and test functions can be chosen from different functional spaces. By using the fundamental solution as the test function, accurate numerical results can be obtained, which were reported in previous papers for 2-D problems in isotropic, homogeneous or continuously nonhomogeneous and linear elastic solids under static [Atluri et al. (2000); Sladek et al. (2000); Sellountos et al. (2005)] and dynamic loading conditions [Sladek et al. (2003a,b); Sellountos and Polyzos (2003)], and for 3-D problems in homogeneous and isotropic solids under a static or a dynamic load [Han and Atluri (2004a,b)].

In this paper, the MLPG method with a Heaviside step function as the test functions [Atluri et al. (2003); Atluri (2004); Sladek et al. (2004)] is applied to solve two-dimensional (2-D) piezoelectric problems. The mechanical fields are described by the equations of motion with an inertial term. To eliminate the time-dependence in the governing partial differential equations the Laplace-transform technique is applied to the governing equations, which are satisfied in the Laplace-transformed domain in a weak-form on small fictitious subdomains. If the shape of subdomains has a simple form, numerical integrations over them can be easily carried out. Nodal points are introduced and spread on the analyzed domain and each node is surrounded by a small circle for simplicity, but without loss of generality. The integral equations have a very simple nonsingular form. The spatial variations of the displacements and the electric potential are approximated by the Moving Least-Squares (MLS) scheme [Belytschko et al. (1996); Zhu et al. (1998)]. After performing the spatial integrations, a system of linear algebraic equations for unknown nodal values is obtained. The boundary conditions on the global boundary are satisfied by the collocation of the MLS-approximation expressions for the displacements and the electric potential at the boundary nodal points. The Stehfest's inversion method [Stehfest (1970)] is applied to obtain the final time-dependent solutions. The accuracy and the efficiency of the proposed MLPG method are verified by numerical examples.

2 Local boundary integral equations

The governing equations for a homogeneous and linear piezoelectric solid can be derived from an appropriate thermodynamical potential given for instance by the electric enthalpy density H as a function of the strain and the electric fields [Tiersten (1969); Parton and Kudryavtsev (1988)]

$$H(\varepsilon_{ij}, E_j) = \frac{1}{2}c_{ijkl}\varepsilon_{ij}\varepsilon_{kl} - e_{jkl}E_j\varepsilon_{kl} - \frac{1}{2}h_{jk}E_jE_k, \quad (1)$$

where c_{ijkl}, e_{jkl} and h_{jk} are elastic, piezoelectric and dielectric material tensors, respectively. The strain tensor ε_{ij} and the electric field vector E_j are related to the displacements u_i and the electric potential ψ by

$$\varepsilon_{ij} = \frac{1}{2}\left(u_{i,j} + u_{j,i}\right),$$

$$E_j = -\psi_{,j}. \quad (2)$$

Differentiating eq. (1) with respect to ε_{ij} and E_j, one obtains the following constitutive equations for the stress tensor

$$\sigma_{ij} = \frac{\partial H}{\partial \varepsilon_{ij}} = c_{ijkl}\varepsilon_{kl} - e_{kij}E_k, \quad (3)$$

and the electric displacement vector

$$D_j = -\frac{\partial H}{\partial E_j} = e_{jkl}\varepsilon_{kl} + h_{jk}E_k. \quad (4)$$

In many cases, piezoelectric solids are transversely isotropic with $\varepsilon_{33} = \varepsilon_{31} = \varepsilon_{32} = E_3 = 0$ for plane strain conditions. In such a case the constitutive equations (3) and (4) are reduced to [Sheng and Sze (2006)]

$$\begin{aligned}
\begin{bmatrix} \sigma_{11} \\ \sigma_{22} \\ \sigma_{12} \end{bmatrix} &= \begin{bmatrix} c_{11} & c_{12} & 0 \\ c_{12} & c_{22} & 0 \\ 0 & 0 & c_{44} \end{bmatrix} \begin{bmatrix} \varepsilon_{11} \\ \varepsilon_{22} \\ 2\varepsilon_{12} \end{bmatrix} \\
&\quad - \begin{bmatrix} 0 & e_{21} \\ 0 & e_{22} \\ e_{15} & 0 \end{bmatrix} \begin{bmatrix} E_1 \\ E_2 \end{bmatrix} \\
&= \mathbf{C} \begin{bmatrix} \varepsilon_{11} \\ \varepsilon_{22} \\ 2\varepsilon_{12} \end{bmatrix} - \mathbf{L} \begin{bmatrix} E_1 \\ E_2 \end{bmatrix}, \quad (5)
\end{aligned}$$

$$\begin{aligned}
\begin{bmatrix} D_1 \\ D_2 \end{bmatrix} &= \begin{bmatrix} 0 & 0 & e_{15} \\ e_{21} & e_{22} & 0 \end{bmatrix} \begin{bmatrix} \varepsilon_{11} \\ \varepsilon_{22} \\ 2\varepsilon_{12} \end{bmatrix} \\
&\quad + \begin{bmatrix} h_{11} & 0 \\ 0 & h_{22} \end{bmatrix} \begin{bmatrix} E_1 \\ E_2 \end{bmatrix} \\
&= \mathbf{G} \begin{bmatrix} \varepsilon_{11} \\ \varepsilon_{22} \\ 2\varepsilon_{12} \end{bmatrix} + \mathbf{H} \begin{bmatrix} E_1 \\ E_2 \end{bmatrix}, \quad (6)
\end{aligned}$$

where

$$\mathbf{C} = \begin{bmatrix} E_{11}/e & E_{22}\nu_{12}/e & 0 \\ E_{22}\nu_{12}/e & E_{22}/e & 0 \\ 0 & 0 & G_{12} \end{bmatrix} \quad \text{with} \quad e = 1 - \frac{E_{22}}{E_{11}}(\nu_{12})^2,$$

in which E_{11} and E_{22} are Young's modulii, G_{12} is the shear modulus, and ν_{12} is Poisson ratio.

The equations of motion for the mechanical filed and Maxwell's equations for the quasi-static electric field in the analyzed domain Ω can be written as

$$\sigma_{ij,j} - \rho\ddot{u}_i + X_i = 0, \tag{7}$$

$$D_{j,j} = 0 \quad, \tag{8}$$

where X_i is the body force vector, ρ is the mass density and the dots over a quantity indicate the time derivatives. A static problem can be considered formally as a special case of the dynamical one, with omitting the acceleration $\ddot{u}_i(\mathbf{x},t)$ in the equations of motion (7). Therefore, both cases are analyzed simultaneously in this paper.

The following essential and natural boundary conditions are assumed for the mechanical quantities

$$u_i(\mathbf{x},t) = \tilde{u}_i(\mathbf{x},t) \text{on} \; \Gamma_u,$$

$$t_i(\mathbf{x},t) = \tilde{t}_i(\mathbf{x},t) \text{ on } \Gamma_t,$$

and for the electrical quantities

$$\psi(\mathbf{x},t) = \tilde{\psi}(\mathbf{x},t) \text{on} \; \Gamma_p,$$

$$n_i D_i(\mathbf{x},t) = \tilde{Q}(\mathbf{x},t) \text{ on } \Gamma_q,$$

where Γ_u is the part of the global boundary with pre-scribed displacements, and on Γ_t, Γ_p and Γ_q the traction vector, the electric potential and the surface charge density are prescribed, respectively.

Only initial conditions for the mechanical quantities are required, since there is no time derivative of the electrical field according to the quasi-electrostatic assumption. Thus

$$u_i(\mathbf{x},t)|_{t=0} = u_i(x,0) \text{and} \; \dot{u}_i(\mathbf{x},t)|_{t=0} = \dot{u}_i(x,0) \text{ in } \Omega.$$

Applying the Laplace-transform to the governing equations (7), we obtain

$$\overline{\sigma}_{ij,j}(\mathbf{x},p) - \rho p^2\overline{u}_i(\mathbf{x},p) = -\overline{F}_i(\mathbf{x},p), \tag{9}$$

where

$$\overline{F}_i(\mathbf{x},p) = \overline{X}_i(\mathbf{x},p) + pu_i(\mathbf{x},0) + \dot{u}_i(\mathbf{x},0)$$

is the redefined body force in the Laplace-transformed domain with initial boundary conditions for the displacements $u_i(\mathbf{x},0)$ and the velocities $\dot{u}_i(\mathbf{x},0)$.

The Laplace-transform of a function $f(\mathbf{x},t)$ is defined as

$$L[f(x,t)] = \overline{f}(x,p) = \int_0^\infty f(x,t)e^{-pt}dt,$$

where p is the Laplace-transform parameter.

Instead of writing the global weak-form for the above governing equations, the MLPG method constructs a weak-form over the local fictitious subdomains such as Ω_s, which is a small region taken for each node inside the global domain [Atluri (2004)]. The local subdomains overlap each other, and cover the whole global domain Ω. The local subdomains could be of any geometrical shape and size. In the present paper, the local subdomains are taken to be of circular shape. The local weak-form of the governing equations (9) can be written as

$$\int_{\Omega_s} \left[\overline{\sigma}_{ij,j}(\mathbf{x},p) - \rho p^2\overline{u}_i(\mathbf{x},p) + \overline{F}_i(\mathbf{x},p)\right] u_i^*(\mathbf{x}) \, d\Omega = 0, \tag{10}$$

where $u_i^*(\mathbf{x})$ is a test function.

Using

$$\overline{\sigma}_{ij,j}u_i^* = (\overline{\sigma}_{ij}u_i^*)_{,j} - \overline{\sigma}_{ij}u_{i,j}^*$$

and applying the Gauss divergence theorem one can write

$$\int_{\partial\Omega_s} \overline{\sigma}_{ij}(\mathbf{x},p)n_j(\mathbf{x})u_i^*(\mathbf{x})d\Gamma - \int_{\Omega_s} \overline{\sigma}_{ij}(\mathbf{x},p)u_{i,j}^*(\mathbf{x})d\Omega$$

$$+ \int_{\Omega_s} \left[-\rho p^2\overline{u}_i(\mathbf{x},p) + \overline{F}_i(\mathbf{x},p)\right] u_i^*(\mathbf{x})d\Omega = 0, \tag{11}$$

where $\partial\Omega_s$ is the boundary of the local subdomain which consists of three parts $\partial\Omega_s = L_s \cup \Gamma_{st} \cup \Gamma_{su}$ [Atluri (2004)]. L_s is the local boundary that is totally inside the global domain, Γ_{st} is the part of the local boundary which coincides with the global traction boundary, i.e., $\Gamma_{st} = \partial\Omega_s \cap \Gamma_t$, and similarly Γ_{su} is the part of the local boundary that coincides with the global displacement boundary, i.e., $\Gamma_{su} = \partial\Omega_s \cap \Gamma_u$.

By choosing a Heaviside step function as the test function $u_i^*(\mathbf{x})$ in each subdomain

$$u_i^*(\mathbf{x}) = \begin{cases} 1 & \text{at } \mathbf{x} \in \Omega_s \\ 0 & \text{at } \mathbf{x} \notin \Omega_s \end{cases}$$

and considering

$$\bar{t}_i(\mathbf{x}, p) = \overline{\sigma}_{ij}(\mathbf{x}, p) n_j(\mathbf{x}),$$

the local weak-form (11) is converted to the following local boundary-domain integral equations

$$\int_{\partial\Omega_s} \bar{t}_i(\mathbf{x}, p) d\Gamma + \int_{\Omega_s} \left[-\rho p^2 \bar{u}_i(\mathbf{x}, p) + \overline{F}_i(\mathbf{x}, p) \right] d\Omega = 0. \tag{12}$$

Rearranging unknown terms on the left hand side we get

$$\int_{L_s+\Gamma_{su}} \bar{t}_i(\mathbf{x}, p) d\Gamma - \int_{\Omega_s} \rho p^2 \bar{u}_i(\mathbf{x}, p) d\Omega$$
$$= -\int_{\Gamma_{st}} \tilde{\tilde{t}}_i(\mathbf{x}, p) d\Gamma - \int_{\Omega_s} \overline{F}_i(\mathbf{x}, p) d\Omega. \tag{13}$$

Equation (13) is recognized as the overall force equilibrium on the subdomain Ω_s. In the case of stationary problems the domain integral on the left hand side of the local boundary-domain integral equations disappears. Then, a pure boundary integral formulation is obtained under the assumption of vanishing body sources and homogeneous initial conditions.

Similarly, the local weak form of the governing equation (8) can be written as

$$\int_{\Omega_s} \overline{D}_{j,j}(\mathbf{x}, p) u^*(\mathbf{x}) d\Omega = 0, \tag{14}$$

where $u^*(\mathbf{x})$ is a test function.

Applying the Gauss divergence theorem to the local weak-form and considering the Heaviside step function for the test function $u^*(\mathbf{x})$ one can obtain

$$\int_{L_s+\Gamma_{sp}} \overline{Q}(\mathbf{x}, p) d\Gamma = -\int_{\Gamma_{sq}} \tilde{\overline{Q}}(\mathbf{x}, p) d\Gamma, \tag{15}$$

where

$$\overline{Q}(\mathbf{x}, p) = \overline{D}_j n_j = \left(e_{jkl} \bar{u}_{k,l} - h_{jk} \overline{\psi}_{,k} \right) n_j.$$

Since mechanical and electrical fields are coupled in the constitutive equations (5) and (6), we have to deal with the Laplace-transforms of both the mechanical and electrical fields simultaneously.

In the MLPG method the test and the trial functions are not necessarily from the same functional spaces. For internal nodes, the test function is chosen as the Heaviside step function with its support on the local subdomain. The trial functions, on the other hand, are chosen to be the moving least-squares (MLS) interpolation over a number of nodes spread within the domain of influence. The approximated functions for the mechanical displacements and the electric potential can be written as [Atluri (2004)]

$$\overline{\mathbf{u}}^h(\mathbf{x}, p) = \mathbf{\Phi}^T(\mathbf{x}) \cdot \hat{\mathbf{u}}(p) = \sum_{a=1}^{n} \phi^a(\mathbf{x}) \hat{\mathbf{u}}^a(p),$$

$$\overline{\psi}^h(\mathbf{x}, p) = \sum_{a=1}^{n} \phi^a(\mathbf{x}) \hat{\psi}^a(p), \tag{16}$$

where the nodal values $\hat{\mathbf{u}}^a(p)$ and $\hat{\psi}^a(p)$ are fictitious parameters for the displacements and the electric potential, respectively and $\phi^a(\mathbf{x})$ is the shape function associated with the node a. The number of nodes n used for the approximation is determined by the weight function $w^a(\mathbf{x})$. A 4th order spline type weight function is applied in the present work

$$w^a(\mathbf{x}) = \begin{cases} 1 - 6\left(\frac{d^a}{r^a}\right)^2 + 8\left(\frac{d^a}{r^a}\right)^3 - 3\left(\frac{d^a}{r^a}\right)^4, & 0 \le d^a \le r^a \\ 0, & d^a \ge r^a \end{cases} \tag{17}$$

where $d^a = \|\mathbf{x} - \mathbf{x}^a\|$ and r^a is the size of the support domain. It is seen that the C^1-continuity is ensured over the entire domain, therefore the continuity conditions of the tractions and the electric charge are satisfied.

The traction vectors $\bar{t}_i(\mathbf{x}, p)$ at a boundary point $\mathbf{x} \in \partial\Omega_s$ are approximated in terms of the same nodal values $\hat{\mathbf{u}}^a(p)$ as

$$\bar{\mathbf{t}}^h(\mathbf{x}, p) = \mathbf{N}(\mathbf{x})\mathbf{C} \sum_{a=1}^{n} \mathbf{B}^a(\mathbf{x})\hat{\mathbf{u}}^a(p) + \mathbf{N}(\mathbf{x})\mathbf{L} \sum_{a=1}^{n} \mathbf{P}^a(\mathbf{x})\hat{\psi}^a(p), \tag{18}$$

where the matrix $\mathbf{N}(\mathbf{x})$ is related to the normal vector $\mathbf{n}(\mathbf{x})$ on $\partial\Omega_s$ by

$$\mathbf{N}(\mathbf{x}) = \begin{bmatrix} n_1 & 0 & n_2 \\ 0 & n_2 & n_1 \end{bmatrix},$$

and the matrices $\mathbf{B}^a$ and $\mathbf{P}^a$ are represented by the gradients of the shape functions as

$$\mathbf{B}^a = \begin{bmatrix} \phi^a_{,1} & 0 \\ 0 & \phi^a_{,2} \\ \phi^a_{,2} & \phi^a_{,1} \end{bmatrix}, \quad \mathbf{P}^a = \begin{bmatrix} \phi^a_{,1} \\ \phi^a_{,2} \end{bmatrix}.$$

Similarly the electrical charge $\overline{Q}(\mathbf{x},p)$ can be approximated by

$$\overline{Q}^h(\mathbf{x},p) = \mathbf{N}_1(\mathbf{x})\mathbf{G}\sum_{a=1}^n \mathbf{B}^a(\mathbf{x})\hat{\mathbf{u}}^a(p)$$
$$- \mathbf{N}_1(\mathbf{x})\mathbf{H}\sum_{a=1}^n \mathbf{P}^a(\mathbf{x})\hat{\psi}^a(p), \tag{19}$$

where the matrices $\mathbf{G}$ and $\mathbf{H}$ are defined in eq. (6) and

$$\mathbf{N}_1(\mathbf{x}) = \begin{bmatrix} n_1 & n_2 \end{bmatrix}.$$

Obeying the boundary conditions at those nodal points on the global boundary, where the displacements and the electrical potential are prescribed, and making use of the approximation formula (16), one obtains the discretized form of the boundary conditions as

$$\sum_{a=1}^n \phi^a(\zeta)\hat{\mathbf{u}}^a(p) = \tilde{\overline{\mathbf{u}}}(\zeta,p) \quad \text{for } \zeta \in \Gamma_u, \tag{20}$$

$$\sum_{a=1}^n \phi^a(\zeta)\hat{\psi}^a(p) = \tilde{\overline{\psi}}(\zeta,p) \quad \text{for } \zeta \in \Gamma_p. \tag{21}$$

Furthermore, in view of the MLS-approximation (18) and (19) for the unknown quantities in the local boundary-domain integral equations (13) and (15), we obtain their discretized forms as

$$\sum_{a=1}^n \left(\int_{L_s+\Gamma_{su}} \mathbf{N}(\mathbf{x})\mathbf{CB}^a(\mathbf{x})d\Gamma - \mathbf{I}\rho p^2 \int_{\Omega_s} \phi^a(\mathbf{x})d\Omega \right) \hat{\mathbf{u}}^a(p)$$
$$+ \sum_{a=1}^n \left(\int_{L_s+\Gamma_{su}} \mathbf{N}(\mathbf{x})\mathbf{LP}^a(\mathbf{x})d\Gamma \right) \hat{\psi}^a(p)$$
$$= -\int_{\Gamma_{st}} \tilde{\overline{\mathbf{t}}}(\mathbf{x},p)d\Gamma - \int_{\Omega_s} \overline{\mathbf{F}}(\mathbf{x},p)d\Omega, \tag{22}$$

$$\sum_{a=1}^n \left(\int_{L_s+\Gamma_{sp}} \mathbf{N}_1(\mathbf{x})\mathbf{GB}^a(\mathbf{x})d\Gamma \right) \hat{\mathbf{u}}^a(p)$$
$$- \sum_{a=1}^n \left(\int_{L_s+\Gamma_{sp}} \mathbf{N}_1(\mathbf{x})\mathbf{HP}^a(\mathbf{x})d\Gamma \right) \hat{\psi}^a(p)$$
$$= -\int_{\Gamma_{sq}} \tilde{\overline{Q}}(\mathbf{x},p)d\Gamma, \tag{23}$$

which are considered on the sub-domains adjacent to interior nodes as well as to the boundary nodes on Γ_{st} and Γ_{sq}. In eq. (22), $\mathbf{I}$ is a unit matrix defined by

$$\mathbf{I} = \begin{pmatrix} 1 & 0 \\ 0 & 1 \end{pmatrix}.$$

Collecting the discretized local boundary-domain integral equations together with the discretized boundary conditions for the displacements and the electric potential, we get the complete system of linear algebraic equations for the computation of nodal unknowns which are the Laplace-transforms of the fictitious parameters $\hat{\mathbf{u}}^a(p)$ and $\hat{\psi}^a(p)$. The time dependent values of the transformed quantities can be obtained by an inverse Laplace-transform. There are many inversion methods available for the Laplace-transform. In the present analysis the Stehfest algorithm [Stehfest (1970)] is used.

3 Numerical examples

In this section numerical results for the bending of a square piezoelectric panel are presented to illustrate the accuracy of the proposed method. The square panel with a size $a \times a = 1mm \times 1mm$ made of a PZT-4 material is subjected to a pure bending moment arising from a linearly varying stress at the right boundary (Fig. 1). The lower boundary of the panel is earthed with a vanishing electrical potential. Other boundaries have prescribed vanishing electrical charge.

The material coefficients corresponding to PZT-4 material are following

$$c_{11} = 13.9 \cdot 10^{10} Nm^{-2}, \quad c_{12} = 7.43 \cdot 10^{10} Nm^{-2},$$

$$c_{22} = 11.3 \cdot 10^{10} Nm^{-2}, \quad c_{44} = 2.56 \cdot 10^{10} Nm^{-2},$$

$$e_{15} = 13.44 Cm^{-2}, \quad e_{21} = -6.98 Cm^{-2},$$
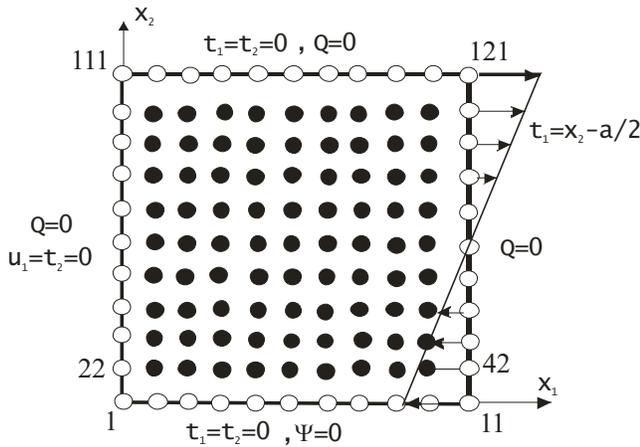
$$e_{22} = 13.84 Cm^{-2},$$

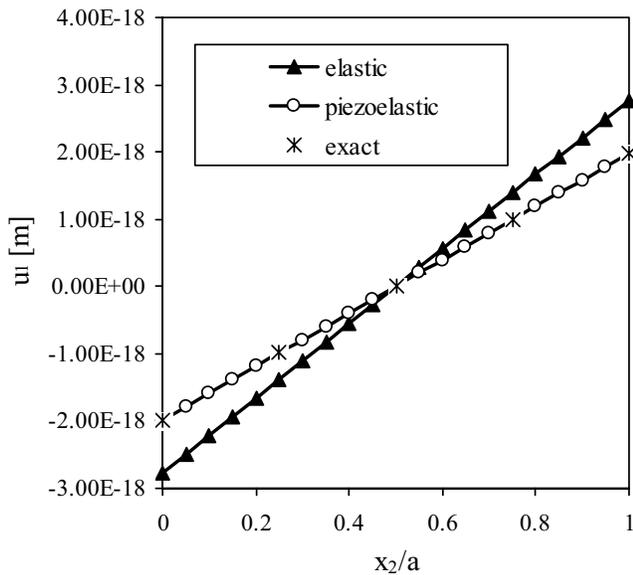**Figure 1** : Bending of a square piezoelectric panel

Figure 2 : Variation of the mechanical displacement u_1 with normalized coordinate x_2/a

$$h_{11} = 6.0 \cdot 10^{-9} C(Vm)^{-1}, \quad h_{22} = 5.47 \cdot 10^{-9} C(Vm)^{-1}.$$

The mechanical displacement and the electrical potential fields on the finite square panel are approximated by using 121 (11x11) nodes equidistantly distributed. The local subdomains are considered to be circular with a radius $r_{loc} = 0.08mm$. First, static boundary conditions are considered.

Numerical results for the components of the mechanical displacements along the line $x_1 = a/2$ are presented in Figs. 2 and 3. The analytical solution of the problem is given by Parton et al. (1989). One can observe an excel-

Figure 3 : Variation of the mechanical displacement u_2 with normalized coordinate x_2/a

lent agreement of the present results with the exact solution. To see the influence of the electrical field on the mechanical displacements the results for a pure elastic panel ($e_{15} = e_{21} = e_{22} = 0$) are given too. For the considered boundary conditions, the mechanical displacement component u_1 is increased or reduced depending on the position considered, while mechanical displacement component u_2 is reduced in the piezoelectric panel compared to a pure elastic one.

Numerical results for the displacement component u_2 and the electric potential along the line $x_2 = a/2$ are given in Figs. 4 and 5. Again one can observe an excellent agreement of the present results and the exact solution in the whole interval considered.

The relative percentage errors and the convergence rates for three different node distributions are presented in Fig. 6, where s represents the node-distance for regular node distributions. The relative errors are computed for u_2 and ψ at the center of the panel $x_1 = x_2 = a/2$. Coarser and finer node distributions are considered with respect to previous numerical calculations with 121 nodes. The total number of boundary and internal nodes in the coarse distribution is 30 and in the fine one it is 441.

In the next example, we consider the same piezoelectric panel subject to an impact load with Heaviside time variation. Both the geometrical and the material parameters are the same as in the previous static case. For the nu-
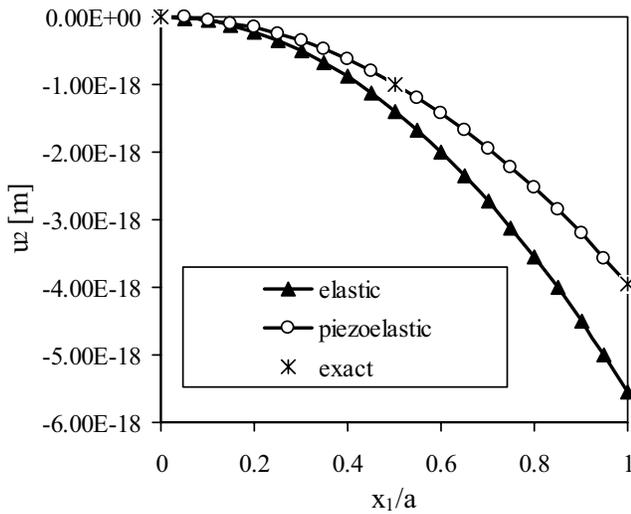
Figure 4 : Variation of the mechanical displacement u_2 with normalized coordinate x_1/a
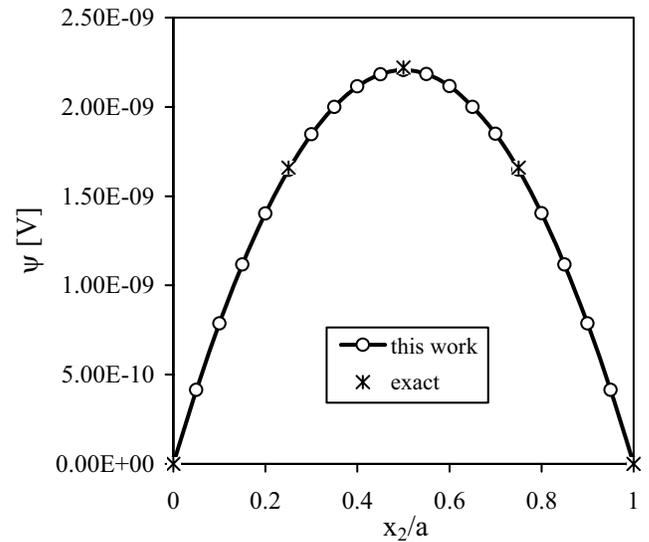

Figure 5 : Variation of the electrical potential with normalized coordinate x_2/a
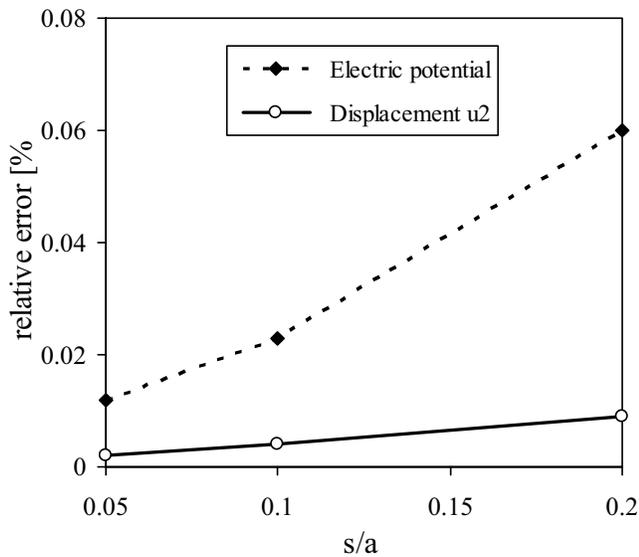

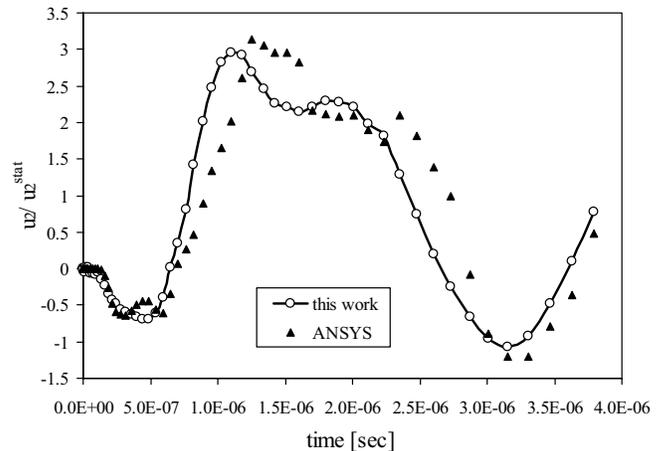**Figure 6** : Relative errors and convergence rates

Figure 7 : Time variation of the displacement u_2 at the center of the panel

merical calculations we have used again 441 nodes with a regular distribution.

The time variations of the normalized displacement component u_2/u_2^{stat} and the normalized electric potential ψ/ψ^{stat} at the center of the panel are given in Figs. 7 and 8, which are compared with those obtained by the FEM-ANSYS computer code. The FEM results have been obtained by using 3600 quadratic eight-noded elements with1000 time increments. A good agreement between both results is achieved, which verifies the accuracy of the present meshless method. The static dis-

placement and the static electric potential at the center of the panel are $u_2^{stat} = -0.990228 \cdot 10^{-18} m$ and $\psi^{stat} = 0.22223 \cdot 10^{-8} V$, respectively.

4 Conclusions

A meshless local Petrov-Galerkin method (MLPG) is presented for plane piezoelectricity. Both static and impact loads are considered. The Laplace-transform technique is applied to eliminate the time variable in the coupled governing partial differential equations. The analyzed domain is divided into small overlapping circu-
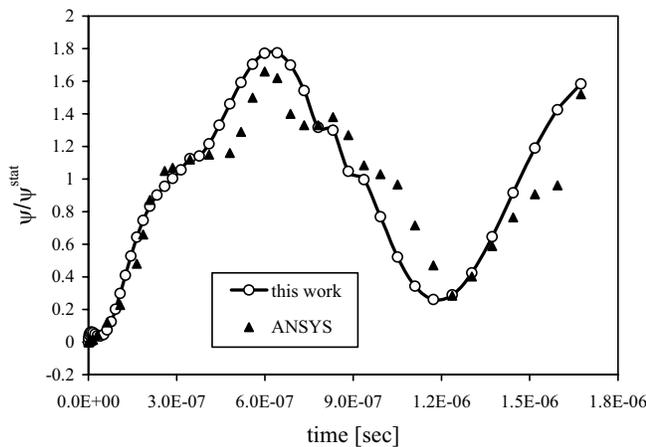
Figure 8 : Time variation of the electric potential at the center of the panel

lar subdomains. A unit step function is used as the test functions in the local weak-form. The derived local boundary-domain integral equations are nonsingular. The moving least-squares (MLS) scheme is adopted for approximating the physical quantities. The proposed method is a truly meshless method, which requires neither domain elements nor background cells in either the interpolation or the integration.

The present method is an alternative numerical tool to many existing computational methods like FEM or BEM. The main advantage of the present method is its simplicity. Contrary to the conventional BEM, the resent method requires no fundamental solutions and all integrands in the present formulation are regular. Thus, no special numerical techniques are required to evaluate the integrals. The present formulation possesses the generality of the FEM. Therefore, the method is promising for numerical analysis of multi-field problems like piezoelectric or thermoelastic problems, which cannot be solved effectively by the conventional BEM. Moreover, the present meshless method seems to be more flexible than the standard FEM, since an adaptation of the nodal density is easier than a mesh adaptation.

References

Atluri, S.N. (2004): The Meshless Method, (MLPG) For Domain & BIE Discretizations, Tech Science Press.

Atluri, S.N.; Sladek, J.; Sladek, V.; Zhu, T. (2000): The local boundary integral equation (LBIE) and its meshless implementation for linear elasticity. Comput. Mech., 25: 180-198.

Atluri, S.N.; Han, Z.D.; Shen, S. (2003): Meshless local Petrov-Galerkin (MLPG) approaches for solving the weakly-singular traction & displacement boundary integral equations. CMES: Computer Modeling in Engineering & Sciences, 4: 507-516.

Belytschko, T.; Krogauz, Y.; Organ, D.; Fleming, M.; Krysl, P. (1996): Meshless methods; an overview and recent developments. Comp. Meth. Appl. Mech. Engn., 139: 3-47.

Chen, T.; Lin, F.Z. (1995): Boundary integral formulations for three-dimensional anisotropic piezoelectric solids. Computational Mechanics, 15: 485-496.

Ding, H.; Liang, J. (1999): The fundamental solutions for transversaly isotropic piezoelectricity and boundary element method. Computers & Structures, 71: 447-455.

Enderlein, M.; Ricoeur, A.; Kuna, M. (2005): Finite element techniques for dynamic crack analysis in piezoelectrics. International Journal of Fracture, 134: 191-208.

Garcia-Sanchez, F.; Saez, A.; Dominguez, J. (2005): Anisotropic and piezoelectric materials fracture analysis by BEM. Computers & Structures, 83: 804-820.

Garcia-Sanchez, F.; Zhang, Ch.; Sladek, J.; Sladek, V. (2006): 2-D transient dynamic crack analysis in piezoelectric solids by BEM. Computational Materials Science, in press.

Gaudenzi, P.; Bathe, K.J. (1995): An iterative finite element procedure for the analysis of piezoelectric continua. Journal of Intelligent Material Systems and Structures, 6: 266-273.

Gross, D.; Rangelov, T.; Dineva, P. (2005): 2D wave scattering by a crack in a piezoelectric plane using traction BIEM. SID: Structural Integrity & Durability, 1: 35-47.

Ha, S.K.; Keilers, C.; Chang, F.K. (1992): Finite element analysis of composite structures containing distributed piezoceramic sensors and actuators. AIAA Journal, 30: 772-780.

Han, Z.D.; Atluri, S.N. (2004a): Meshless local Petrov-Galerkin (MLPG) approaches for solving 3D problems in elasto-statics. CMES: Computer Modeling in Engineering & Sciences, 6: 169-188.

Han, Z.D.; Atluri, S.N. (2004b): A meshless local Petrov-Galerkin (MLPG) approach for 3-dimensional elasto-dynamics. CMC: Computers, Materials & Continua, 1: 129-140.

Lee, J.S. (1995): Boundary element method for electroelastic interaction in piezoceramics. Engineering Analysis with Boundary Elements, 15: 321-328.

Liu, G.R.; Dai, K.Y.; Lim, K.M.; Gu, Y.T. (2002): A point interpolation mesh free method for static and frequency analysis of two-dimensional piezoelectric structures. Computational Mechanics, 29: 510-519.

Ohs, R.R.; Aluru, N.R. (2001): Meshless analysis of piezoelectric devices. Computational Mechanics, 2**7**: 23-36.

Pan, E. (1999): A BEM analysis of fracture mechanics in 2D anisotropic piezoelectric solids. Engineering Analysis with Boundary Elements, 23: 67-76.

Parton, V.Z.; Kudryavtsev, B.A. (1988): Electromagnetoelasticity, Piezoelectrics and Electrically Conductive Solids, Gordon and Breach Science Publishers, New York.

Parton, V.Z.; Kudryavtsev, B.A.; Senik, N.A. (1989): Electroelasticity. Applied Mechanics: Soviet Review, 2: 1-58.

Sellountos, E.J.; Polyzos, D. (2003): A MLPG (LBIE) method for solving frequency domain elastic problems. CMES: Computer Modeling in Engineering & Sciences, 4: 619-636.

Sellountos, E.J.; Vavourakis, V.; Polyzos, D. (2005): A new singular/hypersingular MLPG (LBIE) method for 2D elastostatics. CMES: Computer Modeling in Engineering & Sciences, 7: 35-48.

Sheng, N.; Sze, K.Y. (2006): Multi-region Trefftz boundary element method for fracture analysis in plane piezoelectricity. Computational Mechanics, 37: 381-393.

Sladek, J.; Sladek, V.; Atluri, S.N. (2000): Local boundary integral equation (LBIE) method for solving problems of elasticity with nonhomogeneous material properties. Computational Mechanics, 24: 456-462.

Sladek, J.; Sladek, V.; Van Keer, R. (2003a): Meshless local boundary integral equation method for 2D elastodynamic problems. Int. J. Num. Meth. Engn., 57: 235-249

Sladek, J.; Sladek, V.; Zhang, Ch. (2003b): Application of meshless local Petrov-Galerkin (MLPG) method to elastodynamic problems in continuously nonhomogeneous solids. CMES: Computer Modeling in Engn. & Sciences, 4: 637-648.

Sladek, J.; Sladek, V.; Atluri, S.N. (2004): Meshless local Petrov-Galerkin method in anisotropic elasticity. CMES: Computer Modeling in Engn. & Sciences, 6: 477-489.

Stehfest, H. (1970): Algorithm 368: numerical inversion of Laplace transform. Comm. Assoc. Comput. Mach., 13: 47-49.

Tiersten, H.F. (1969): Linear Piezoelectric Plate Vibrations, Plenum Press, New York.

Zhu, T.; Zhang, J.D.; Atluri, S.N. (1998): A local boundary integral equation (LBIE) method in computational mechanics, and a meshless discretization approaches. Computational Mechanics, 21: 223-235.